J Solid State Electrochem (2011) 15:1057–1062
DOI 10.1007/s10008-011-1317-8

ORIGINAL PAPER

Durability investigation of graphene-supported Pt nanocatalysts for PEM fuel cells

Huimin Wu · David Wexler · Huakun Liu

Received: 16 December 2010 / Revised: 10 January 2011 / Accepted: 14 January 2011 / Published online: 8 February 2011
© Springer-Verlag 2011

Abstract We report graphene nanosheets as a durable alternative support material for Pt nanoparticle catalysts for oxygen reduction in proton exchange membrane (PEM) fuel cells and compared them to XC-72. The materials were characterized by X-ray diffraction and transmission electron microscopy. Electrochemical surface oxidation of XC-72 and graphene, and of Pt/XC-72 and Pt/graphene has been compared following treatments for up to 120 h. The electrochemical performance of the specimens was evaluated by cyclic voltammetry and linear sweep voltammetry at different surface oxidation time intervals. Electrochemical measurements indicate that the graphene exihibits greatly enhanced electrochemical durability. It is suggested that graphene nanosheet is a promising, low-cost, and durable electrocatalyst support for oxygen reduction in the PEM fuel cell.

Keywords Oxygen reduction · Durability · Graphene · PEM fuel cell · Carbon black

Introduction

Proton exchange membrane fuel cells (PEMFCs) are the most promising candidates for transportation applications due to their low operating temperature (<100 °C) and fast start-up [1–3]. The durability of the PEM fuel cell has been recently recognized as one of the most important issues to be addressed before the commercialization of PEMFCs [4–6].

In the state-of-the-art PEM fuel cell, platinum on carbon (Pt/XC-72) is widely used as an electrocatalyst in low-temperature fuel cells due to its excellent reaction kinetics at low temperature [7]. Despite its widespread use, carbon can be electrochemically oxidized to surface oxides, and eventually to CO_2 at the cathode under PEM fuel cell conditions, which leads to Pt nanoparticle sintering on or detachment from the support material and degrades fuel cell performance [8]. Therefore, much effort has been devoted to developing durable catalyst support materials [9], carbon nanotubes (CNT) [10–13] and mesoporous carbon (MPC) [14], for example. However, both CNTs and MPC have the issue of high cost.

Recently, graphene, a single layer of carbon [carbon atoms in a two-dimensional (2D) honeycomb lattice] was found to exist as a free-standing form and exhibits many unusual and intriguing physical, chemical, and mechanical properties. Due to the high quality of the sp2 carbon lattice, electrons were found to move ballistically in graphene layer even at ambient temperature. Furthermore, graphene was exfoliated from graphite. Graphite is abundant and cheap. So, graphene has attracted strong scientific and technological interest [15] with great application potentials in various fields, such as electronic devices [16], nanocomposites [17–19], sustainable energy storage and conversion [20, 21], batteries [22], and fuel cells [23–26]. It has been proposed that carbon materials with a higher graphite component could be more stable [13].

In this study, we compare the electrochemical properties of graphene with XC-72, and it is found that the use of graphene can be promising in effectively reducing the carbon corrosion problem.

H. Wu (✉)
Hubei University, College of Chemistry & Chemical Engineering,
Wuhan 430062, People's Republic of China
e-mail: whm267@gmail.com

H. Liu
e-mail: hua@uow.edu.au

H. Wu · D. Wexler · H. Liu (✉)
Institute for Superconducting & Electronic Materials,
School of Mechanical, Materials and Mechatronics Engineering,
University of Wollongong,
Wollongong, NSW 2522, Australia

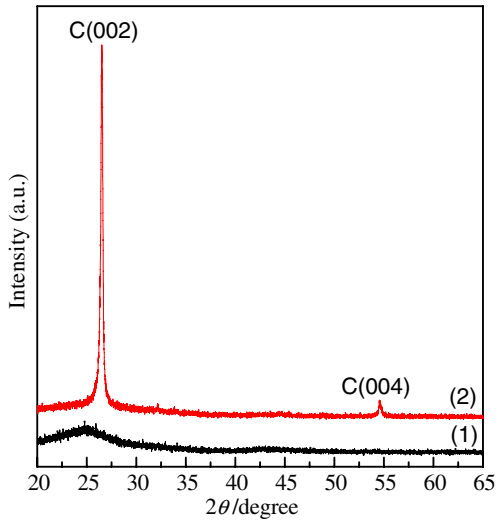

Fig. 1 X-ray diffraction patterns of (**a**) XC-72 and (**b**) graphene

Experimental

Materials preparation

All chemicals were American Chemical Society standard (ACS) reagents and purchased from Sigma-Aldrich. Graphene nanosheets were synthesized by the method reported in [27]. The deposition of Pt on graphene was realized by a similar reported chemical method [28]. Typically, H_2PtCl_6•$6H_2O$ was dissolved in deionized water. Then, an appropriate amount of graphene was added to the solution, so as to achieve a Pt-to-C weight ratio of 20:80, and dispersed by ultrasonic probe for about 0.5 h. After that, 10 mL aqueous solution of $NaBH_4$ was added dropwise into the mixture to achieve reduction under Ar atmosphere. The reacting dispersion was stirred and refluxed continuously for at least 30 min. Finally, the black dispersion was isolated by centrifugation and washed 3–4 times with ethanol. The black powder was then dried at 60 °C in a vacuum oven overnight. As a comparison, the electrochemical performance of commercial BASF Pt/C catalyst (20% Pt supported on XC-72 carbon, BASF Chemical) was also examined. So, all the references to Pt/XC-72 catalyst throughout this report are to commercial BASF Pt/C catalyst.

Physical characterization

The phases identities of the XC-72 and graphene were characterized by X-ray diffraction (XRD), using a GBC MMA X-ray diffractometer with CuKα radiation. The Pt morphologies and nanostructures before and after oxidation treatments were analyzed by transmission electron microscopy (TEM) and high resolution TEM using a JEOL JEM 2011 TEM instrument. TEM specimens were prepared by making a suspension in ethanol followed by deposition onto a holey carbon-coated copper grid.

Electrochemical measurements

Electrochemical measurements were performed with a three-electrode configuration. The working electrodes were made by casting the specimen (either XC-72, graphene nanosheets, 20 wt% Pt/XC-72, or 20 wt% Pt/graphene) as a thin film onto a glass carbon rotating disk electrode (geometrical area=0.196 cm^2), with Nafion as the binding agent. The counter electrode was a Pt wire, and the reference electrode was an Ag/AgCl/10% KNO_3 electrode (0.22 V vs. NHE). So, all potentials are measured with respect to the Ag/AgCl/10% KNO_3. The electrolyte

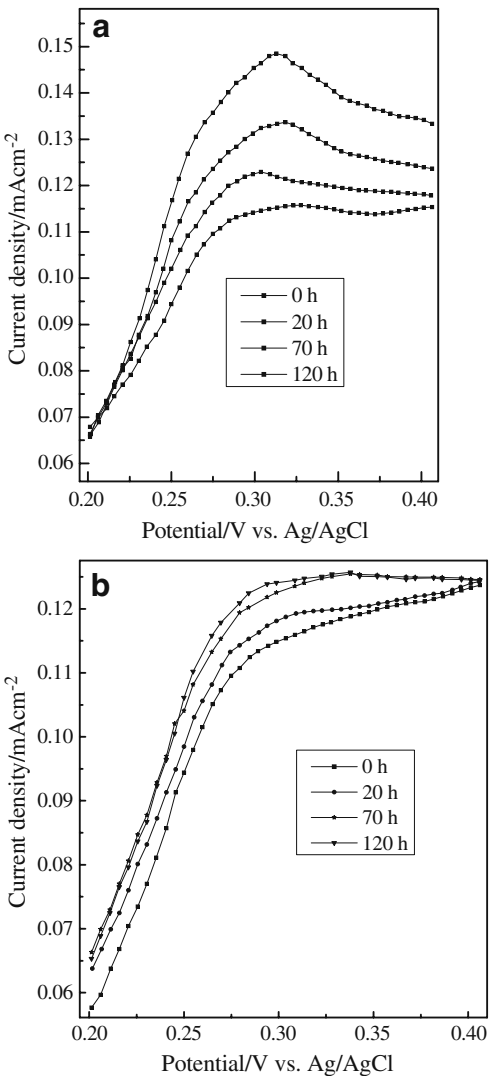

Fig. 2 Forward scan of cyclic voltammgrams of (**a**) XC-72 and (**b**) graphene at different intervals during oxidation treatment in N_2-saturated 0.1 M $HClO_4$; scan rate: 10 mVs^{-1}

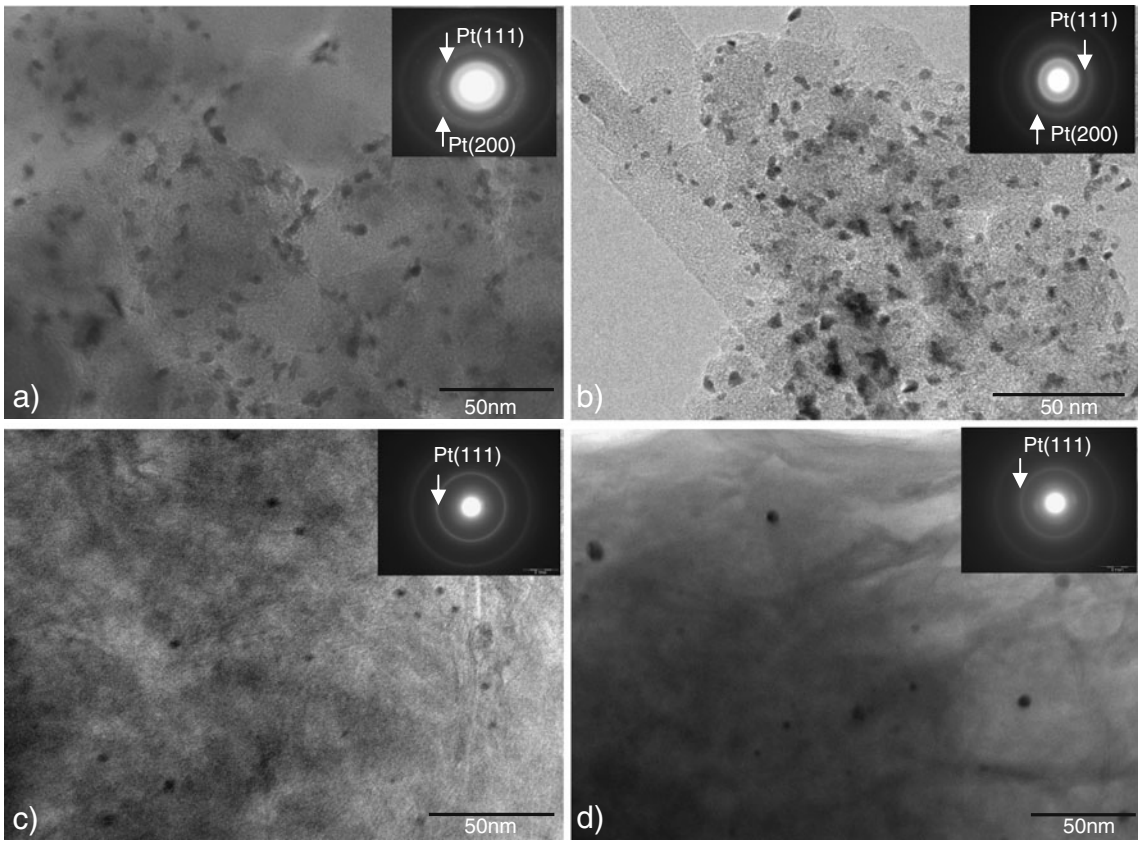

Fig. 3 TEM bright field micrographs of (**a**) Pt/XC-72; (**b**) Pt/XC-72 after oxidation treatment; (**c**) Pt/graphene; and (**d**) Pt/graphene after oxidation treatment; with insets in (**a**), (**b**), (**c**), and (**d**) showing the corresponding selected area electron diffraction patterns

solution was 0.1 mol/L $HClO_4$ [29, 30]. All measurements were performed at room temperature (25 °C).

For the surface oxidation experiments, the working electrode was immersed in N_2-saturated 0.1 M $HClO_4$. A constant potential (0.7 V) was applied [31]. For XC-72 and graphene, throughout the oxidation process, cyclic voltammetry (CV) was conducted at different time intervals from 0.2 to 0.5 V at 10 mVs^{-1} to monitor the surface oxidation. For Pt catalyzed XC-72 or graphene, besides conducting CV from −0.2 to 1.0 V at 50 mVs^{-1} to determine the Pt active surface area, the activity towards the oxygen reduction reaction (ORR) was also examined by potentiodynamic current measurements from 0.9 to 0.2 V at the sweep rate of 10 mV s^{-1} and rotation rate of 1,600 rpm.

Results and discussion

The XRD patterns of XC-72 carbon and graphene are shown in Fig. 1. For XC-72 carbon, a rather wide and shallow (002) peak is observed in its XRD pattern, implying that XC-72 is an amorphous carbon material with small regions of crystallinity. A sharper and narrower carbon (002) diffraction peak appears for graphene, which indicates its highly graphitic ordered structure. The presence of the C (004) diffraction peak in graphene is also indicative of the high crystallinity of its carbon structure [32, 33]. The graphitic structure of carbon can be quantitatively characterized by the graphitization index,

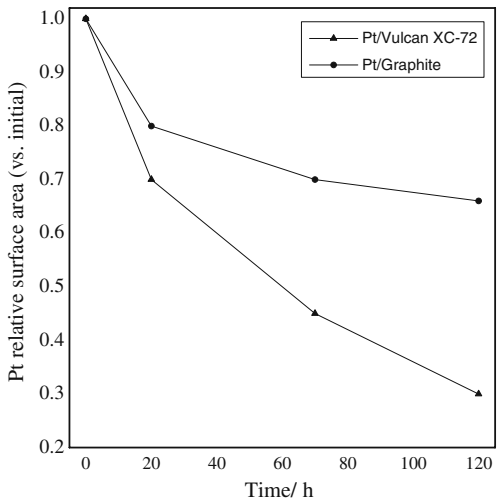

Fig. 4 Comparison of Pt active surface area loss vs. time for XC-72 and graphene

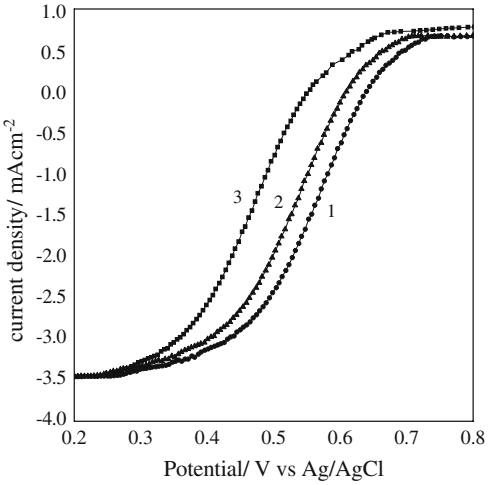

Fig. 5 Linear scan voltammograms on Pt/graphene as a function of oxidation treatment time in 0.1 M $HClO_4$ solution saturated with oxygen. A rotating disk electrode at 1,600 rpm and a scan rate of 10 mV/s were used

which indicates the degree of similarity between a carbon material and a perfect single crystal of graphite [34]. A higher graphitization index indicates a more ordered graphitic structure [35].

Figure 2 shows the forward scan of a cyclic voltammogram for XC-72 and graphene after oxidation treatment for different durations. The current density was calculated based on the geometric electrode area. The peak current comes from the surface oxide formation due to the hydroquinone-quinone redox couple on the surface [31]. Similar results have been reported by Jarvi and coworkers [36], who identified different oxidized groups including carboxyl, hydroxyl, and carbonyl generated on the carbon surface through X-ray photoelectron spectroscopy and thermal gravimetric analysis coupled to mass spectrometry. In Fig. 2a, note that the peak in the hydroquinone-quinone region becomes stronger with treatment time, and the increased peak current suggests a higher degree of surface carbon oxidation with time.

In contrast, the peak current is barely visible in the case of graphene and shows negligible change with time (Fig. 2b), which suggests that the surface of graphene is more difficult to oxidize than XC-72 under the tested conditions. This can be attributed to the graphitic structure of graphene; similar results have been reported in [13]. This means that graphene could potentially be more corrosion resistant and durable when used in a fuel cell.

Figure 3 shows TEM bright field micrographs of the Pt/C before oxidation (Fig. 3a) and after oxidation (Fig. 3b), and of the Pt/graphene before oxidation (Fig. 3c) and after oxidation (Fig. 3d). We performed selected area electron diffraction on the catalysts. We also performed quantitative energy dispersive X-ray analysis on the samples. For each sample, the Pt-to-C weight ratio was equal to the nominal ratio (1:4). The associated spotty ring patterns are shown in the insets in Fig. 3a, b, c, and d, respectively. The bright spots in these correspond to the (111) and (200) Pt reflections, and the additional diffuse rings correspond to amorphous carbon and graphene. The dark nanoparticles are the Pt catalyst. Although the Pt loading levels are the same, the population of Pt nanoparticle is too small for Pt/graphene compared to Pt/XC-72, which maybe can attribute to the structure of the support. Comparison of Fig. 3a and b indicates the effects of oxidation on the general morphology of the Pt/XC-72. In general, the carbon matrix exhibits a fluffy cotton-like microstructure, in which Pt nanoparticles are embedded. Specifically, for the Pt/XC-72 before oxidation, the particles have a particle size in the range of 5–8 nm, and they are also distributed homogeneously on the micrometer domain. After oxidation treatment, the particle size becomes bigger. Furthermore, the Pt particles are aggregated, which will reduce the catalytic activity.

In contrast, for graphene after oxidation treatment, the Pt particle size shows some increase in some regions. However, after oxidation treatment, some aggregation of Pt nanoparticles is indeed observed in some isolated areas on the graphene surface, as opposed to the uniform aggregation in the case of XC-72, and this is attributed to the higher corrosion resistance of graphene, which is consistent with the results deduced from Fig. 2. Comparing Fig. 3a and c, the Pt is better dispersed on the graphene than on the XC-72 carbon, which is attributed to the fact that catalyst nanoparticles could be easily deposited on the surface of graphene based on its 2D flat planes [24].

The working electrode was immersed in N_2-saturated 0.1 M $HClO_4$, and a constant potential (0.7 V) was added. The current response as a function of time was then recorded. To quantify the effects of oxidation treatment on the Pt electrochemically active surface area (ECSA), cyclic voltammetry was performed on Pt/XC-72 and Pt/graphene in N_2-saturated 0.1 M $HClO_4$ electrolyte at different time intervals (0 h, 20 h, 70 h, 120 h). The Pt ECSA was determined by measuring the charges collected in the underpotential hydrogen (H_{upd}) adsorption/desorption region after double-layer correction and assuming a value of

Table 1 Comparison of half potential for ORR between Pt supported on XC-72 and graphene as a function of oxidation treatment time, with a rotation rate of 1,600 rpm

Time (h)	XC-72 (V)	Graphene (V)
0	0.58	0.58
20	0.53	0.55
120	0.45	0.48

210 μC/cm^2 for the adsorption of a hydrogen monolayer [37]. The ECSA values of the catalysts were calculated to be 80.1 m^2/g (Pt/XC-72) and 98 m^2/g (Pt/graphene), respectively. The ECSA accounts not only for the catalyst surface available for charge transfer, but also includes the access to a conductive path to transfer the electrons to and from the electrode surface. The ECSA difference between the two catalysts may be due to the different matrix and the smaller particle size of the Pt loaded on the graphene. High ECSAs are favorable for the electrochemical oxygen reduction reaction.

The loss of Pt surface area with time during the surface oxidation experiments is plotted in Fig. 4. It can be seen that almost 70% of the Pt surface area was lost for XC-72 after 120 h, while only 30% loss is observed for graphene. Furthermore, most of the surface area loss in the case of graphene occurs within 70 h, while after 70 h, the rate of Pt area loss is very small, indicating that graphene could potentially provide much higher durability than XC-72. The loss of Pt surface area supported on XC-72 and graphene could be due to the dissolution of Pt(0) particles, reprecipitation of Pt ions, and diffusion of Pt ions into the membrane [38], while the interactions between Pt(0) and the carbon support material influence the drop in the active surface area of the catalyst. A change in the electronic structure in the platinum catalytic layer from interaction between the platinum active phase and the carbon support phase leads to changes in catalyst durability [39]. Graphene with its unique graphitized basal plane can improve the interaction of Pt precursor with graphene during platinization.

The catalytic activities in terms of the ORR were also examined at different time intervals by linear sweep voltammetry measurements in oxygen-saturated 0.1 mol/L $HClO_4$, as shown in Fig. 5. Although the Pt surface area decreased as the treatment time increased (Fig. 4), there were no changes in the limiting currents. It is believed that at the high voltage bias used, the reaction kinetics is so fast that the process is still diffusion limited even after some significant reduction of Pt surface area. On the other hand, the half wave potential shows a continuous decrease as the treatment time increases and is thus used to quantify the difference in activity. The half wave potential, defined as the potential at which the measured current reaches the half of the limiting current, was extracted from the potentiodynamic curve. As listed in Table 1, Pt supported on XC-72 has a similar initial half wave potential to Pt supported on graphene, but as time goes on, both of them show a decrease in activity as evidenced by the lowering of the half wave potential. However, graphene exhibits a slower decrease rate than XC-72. At the same time, the half wave potential of Pt/graphene is higher than that of Pt/XC-72. The higher performance of the Pt/graphene electrode, compared to the Pt/XC-72 electrode could be attributed to the good accessibility and dispersion of the graphene supports so as to yield sufficient active Pt surface area by helping the dispersion of small Pt particles [40]. This is in agreement with the trend observed for the change in Pt surface area in Fig. 4.

Conclusion

In summary, graphene nanosheets were employed as an alternative support material for Pt nanoparticles for oxygen reduction. The 20 wt% Pt/graphene catalysts were prepared using a simple chemical reduction method and compared to BASF 20 wt% Pt/XC-72. The electrochemical characterizations show that graphene has improved corrosion resistance over XC-72. This is attributed to the intrinsic high graphite component and the enhanced Pt-carbon interaction. It is suggested that graphene nanosheet is a promising, low-cost, and durable electrocatalyst support for oxygen reduction in PEM fuel cell.

References

1. Gottesfeld S, Zawodzinski T (1997) Adv Electrochem Sci Eng 5:195–199
2. Shukla AK, Christensen PA, Hamnett A, Hogarth MP (1995) J Power Sources 55:87–92
3. Jung DH, Lee CH, Kim CS, Shin DR (1998) J Power Sources 71:169–173
4. Xie J, Wood DL, Wayne DM, Zawodzinski TA, Atanassov P, Borup RL (2005) J Electrochem Soc 152:A104–A109
5. Knights SD, Colbow KM, St-Pierre J, Wilkinson DP (2004) J Power Sources 127:127–131
6. Stevens DA, Dahn JR (2005) Carbon 43:179–183
7. Vengatesan S, Kim HJ, Kim SK, Oh IH, Lee SY, Cho E, Ha HY, Lim TH (2008) Electrochim Acta 54:856–861
8. Shao YY, Yin GP, Gao YZ (2007) J Power Sources 171:558–562
9. Shao YY, Liu J, Wang Y, Lin YH (2009) J Mater Chem 19:46–59
10. Wu G, Xu BQ (2007) J Power Sources 174:148–158
11. Shao YY, Yin GP, Gao YZ, Shi PF (2006) J Electrochem Soc 153: A1093–A1097
12. Shao YY, Yin GP, Zhang J, Gao YZ (2006) Electrochim Acta 51:5853–5857
13. Wang JJ, Yin GP, Shao YY, Wang ZB, Gao YZ (2008) J Phys Chem C 112:5784–5789
14. Shao Y, Zhang S, Kou R, Wang X, Wang C, Dai S, Viswanathan V, Liu J, Wang Y, Lin Y (2010) J Power Sources 195:1805–1811
15. Geim AK, Novoselov KS (2007) Nat Mater 6:183–191
16. Hass J, de Heer AW, Conrad EH (2008) J Phys Condens Matter 20:27–31
17. Ramanathan T, Abdala AA, Stankovich S, Dikin DA, Herrera-Alonso M, Piner RD, Adamson DH, Schniepp HC, Chen X, Ruoff RS, Nguyen ST, Aksay IA (2008) Nat Nanotechnol 3:327–331
18. Hendricks TR, Lu J, Drzal LT, Lee I (2008) Adv Mater 20:2008–2012
19. He F, Lau S, Chan HL, Fan F (2009) Adv Mater 21:710–715

20. Stoller MD, Park SJ, Zhu YW, An JH, Ruoff RS (2008) Nano Lett 8:3498–3502
21. Shao YY, Wang J, Engelhard MH, Wang CM, Lin YH (2009) J Mater Chem 20:743–747
22. Yoo E, Kim J, Hosono E, Zhou H, Kudo T, Honma I (2008) Nano Lett 8:2277–2281
23. Si YC, Samulski ET (2008) Chem Mater 20:6792–6797
24. Li YM, Tang LH, Li JH (2009) Electrochem Commun 11:846–849
25. Kou R, Shao YY, Wang DH, Engelhard MH, Kwak JH, Wang J, Viswanathan VV, Wang CM, Lin YH, Wang Y, Aksay IA, Liu J (2009) Electrochem Commun 11:954–957
26. Seger B, Kamat PV (2009) J Phys Chem C 113:7990–7995
27. Wang GX, Shen XP, Yao J, Park J (2009) Carbon 47:2049–2053
28. Wu HM, Wexler D, Wang GX (2009) J Alloys Compd 488:195–199
29. Kim DS, Kim YT (2010) Electrochim Acta 55:3628–3633
30. Li XW, Zhu Y, Zou ZQ, Zhao MY, Li ZL, Zhou Q, Yang H (2009) J Electrochem Soc 156:B1107–B1111
31. Wang X, Li WZ, Chen ZW, Waje M, Yan YS (2006) J Power Sources 158:154–159
32. Shanahan PV, Xu LB, Liang CD, Waje M, Dai S, Yan YS (2008) J Power Sources 185:423–437
33. Kim TW, Park IS, Ryoo R (2003) Angew Chem Int Ed 42:4375–4379
34. Liang CD, Dai S, Guiochon G (2003) Anal Chem 75:4904–4912
35. Shao YY, Zhang S, Wang CM, Nie ZM, Liu J, Wang Y, Lin YH (2010) J Power Sources 195:4600–4605
36. Kangasniemi KH, Condit DA, Tarvi TD (2006) J Electrochem Soc 151:E125
37. Schmidt TJ (1998) J Electrochem Soc 145:2354–2358
38. Ohma A, Suga S, Yamamtoto S, Shinohara K (2007) J Electrochem Soc 154:B757–B761
39. Natarajan SK, Hamelin J (2009) J Electrochem Soc 156:B210–B214
40. Wu HM, Wexler D, Wang GX, Liu HK (2011) Adv Sci Lett 4:1–6